Title
Dual polarized near-field focusing plate for near-field optical focusing in two dimensions

Journal
Optics Express, 19(24)

ISSN
1094-4087

Authors
Hosseini, S. Ali
Campione, Salvatore
Capolino, Filippo

Publication Date
2011-11-15

DOI
10.1364/OE.19.024483

Dual polarized near-field focusing plate for near-field optical focusing in two dimensions

S. Ali Hosseini, Salvatore Campione, and Filippo Capolino*

Department of Electrical Engineering and Computer Science, University of California, Irvine, California 92697, USA
*f.capolino@uci.edu
http://capolino.eng.uci.edu

Abstract: We introduce a dual polarized near-field focusing plate (DP-NFFP) with focusing in two dimensions, designed to operate at the near infrared frequency of 193 THz (λ_0 = 1550 nm). Subwavelength focusing in two dimensions, for both incident polarizations, is achieved at a distance of a quarter wavelength from the DP-NFFP. The design procedure is described in detail and the proposed design could be easily scaled to other working frequencies, from microwave to optics. We show that the use of ideal lossless (i.e., perfect electric conductor) or real lossy (i.e., silver) metals provide with subwavelength focusing at 193 THz, indicating that metal losses do not significantly affect the DP-NFFP performance, and thus confirming the design feasibility at the near-infrared frequency. Results are validated by using two distinct full-wave simulators.

OCIS codes: (180.4243) Near-field microscopy; (050.6624) Subwavelength structures.

References and links

1. M. Born and E. Wolf, *Principles of Optics* (Cambridge University Press, London, 1999).
2. D. R. Smith, J. B. Pendry, and M. C. K. Wiltshire, "Metamaterials and negative refractive index," Science **305**(5685), 788–792 (2004).
3. J. B. Pendry, "Negative refraction makes a perfect lens," Phys. Rev. Lett. **85**(18), 3966–3969 (2000).
4. Smolyaninov II, C. C. Davis, J. Elliott, G. A. Wurtz, and A. V. Zayats, "Super-resolution optical microscopy based on photonic crystal materials," Phys. Rev. B **72**, 085442 (2005).
5. V. Westphal and S. W. Hell, "Nanoscale resolution in the focal plane of an optical microscope," Phys. Rev. Lett. **94**(14), 143903 (2005).
6. J. Pendry, A. Holden, D. Robbins, and W. Stewart, "Magnetism from conductors and enhanced nonlinear phenomena," IEEE Trans. Microwave Theory Techn. **47**(11), 2075–2084 (1999).
7. M. C. K. Wiltshire, J. B. Pendry, I. R. Young, D. J. Larkman, D. J. Gilderdale, and J. V. Hajnal, "Microstructured magnetic materials for RF flux guides in magnetic resonance imaging," Science **291**(5505), 849–851 (2001).
8. M. C. K. Wiltshire, J. V. Hajnal, J. B. Pendry, D. J. Edwards, and C. J. Stevens, "Metamaterial endoscope for magnetic field transfer: near field imaging with magnetic wires," Opt. Express **11**(7), 709–715 (2003).
9. S. Steshenko, F. Capolino, P. Alitalo, and S. A. Tretyakov, "Effective model and investigation of the near-field enhancement and subwavelength imaging properties of multilayer arrays of plasmonic nanospheres," Phys. Rev. E **84**, 016607 (2011).
10. P. A. Belov and M. G. Silveirinha, "Resolution of subwavelength transmission devices formed by a wire medium," Phys. Rev. E Stat. Nonlin. Soft Matter Phys. **73**(5), 056607 (2006).
11. G. V. Eleftheriades, A. K. Iyer, and P. C. Kremer, "Planar negative refractive index media using periodically L-C loaded transmission lines," IEEE Trans. Microwave Theory Techn. **50**(12), 2702–2712 (2002).
12. O. Sydoruk, M. Shamonin, A. Radkovskaya, O. Zhuromskyy, E. Shamonina, R. Trautner, C. J. Stevens, G. Faulkner, D. J. Edwards, and L. Solymar, "Mechanism of subwavelength imaging with bilayered magnetic metamaterials: Theory and experiment," J. Appl. Phys. **101**(7), 073903 (2007).
13. Y. Wang, A. M. H. Wong, L. Markley, A. S. Helmy, and G. V. Eleftheriades, "Plasmonic meta-screen for alleviating the trade-offs in the near-field optics," Opt. Express **17**(15), 12351–12361 (2009).
14. E. A. Ash and G. Nicholls, "Super-resolution aperture scanning microscope," Nature **237**(5357), 510–512 (1972).
15. A. Grbic and G. V. Eleftheriades, "Growing evanescent waves in negative-refractive-index transmission-line media," Appl. Phys. Lett. **82**(12), 1815–1817 (2003).
16. A. Grbic and G. V. Eleftheriades, "Overcoming the diffraction limit with a planar left-handed transmission-line lens," Phys. Rev. Lett. **92**(11), 117403 (2004).
17. L. Markley, A. M. H. Wong, Y. Wang, and G. V. Eleftheriades, "Spatially shifted beam approach to subwavelength focusing," Phys. Rev. Lett. **101**(11), 113901 (2008).

#154036 - $15.00 USD Received 6 Sep 2011; revised 18 Oct 2011; accepted 20 Oct 2011; published 15 Nov 2011

18. A. Grbic, L. Jiang, and R. Merlin, "Near-field plates: subdiffraction focusing with patterned surfaces," Science **320**(5875), 511–513 (2008).
19. G. V. Eleftheriades and A. M. H. Wong, "Holography-inspired screens for sub-wavelength focusing in the near field," IEEE Microw. Wirel. Compon. Lett. **18**(4), 236–238 (2008).
20. L. Markley and G. V. Eleftheriades, "Two-dimensional subwavelength focusing using a slotted meta-screen," IEEE Microw. Wirel. Compon. Lett. **19**(3), 137–139 (2009).
21. L. Markley and G. V. Eleftheriades, "A near-field probe for subwavelength-focused imaging," IEEE Trans. Microwave Theory Techn. **58**(3), 551–558 (2010).
22. M. F. Imani and A. Grbic, "An analytical investigation of near-field plates," Metamaterials (Amst.) **4**(2-3), 104–111 (2010).
23. L. Markley and G. V. Eleftheriades, "Two-dimensional subwavelength-focused imaging using a near-field probe at a lambda/4 working distance," J. Appl. Phys. **107**(9), 093102–093105 (2010).
24. P. Alitalo, C. Simovski, A. Viitanen, and S. Tretyakov, "Near-field enhancement and subwavelength imaging in the optical region using a pair of two-dimensional arrays of metal nanospheres," Phys. Rev. B **74**(23), 235425 (2006).
25. C. R. Simovski, A. J. Viitanen, and S. A. Tretyakov, "Sub-wavelength resolution in linear arrays of plasmonic particles," J. Appl. Phys. **101**(12), 123102 (2007).
26. S. Steshenko, F. Capolino, S. A. Tretyakov, and C. R. Simovski, "Super-resolution and near-field enhancement with layers of resonant arrays of nanoparticles," in *Applications of Metamaterials*, F. Capolino, ed. (CRC Press, Boca Raton, FL, 2009), p. 4.1.
27. S. A. Hosseini, S. Campione, and F. Capolino, "A dual polarized near-field focusing plate at microwave frequencies providing sub-wavelength focusing in two dimensions," in *IEEE Antennas Propag. Symp.* (Spokane, WA, 2011).
28. P. B. Johnson and R. W. Christy, "Optical constants of the noble metals," Phys. Rev. B **6**(12), 4370–4379 (1972).
29. I. El-Kady, M. M. Sigalas, R. Biswas, K. M. Ho, and C. M. Soukoulis, "Metallic photonic crystals at optical wavelengths," Phys. Rev. B **62**(23), 15299–15302 (2000).
30. A. Alù, A. Salandrino, and N. Engheta, "Negative effective permeability and left-handed materials at optical frequencies," Opt. Express **14**(4), 1557–1567 (2006).

1. Introduction

The possibility of overcoming the diffraction limit [1] to achieve super resolution and subwavelength focusing has been at the center of interest for imaging applications (e.g., optical microscopy). This was one of the main reasons that led scientists to engineer artifcial materials (metamaterials) with desired electromagnetic properties suitable for this type of applications [2,3]. Subwavelength resolution can be achieved in different manners: using two dimensional photonic and plasmon-polaritonic crystals [4], or single fluorescent molecules as probes [5], or using arrays of Swiss rolls [6–8] in order to transfer subwavelength information directly from the source to the image plane (pixel-to-pixel imaging principle), 1D and 2D arrays of plasmonic nanospheres [9], anisotropic and hyperbolic materials [10], transmission lines [11], magnetoinductive waves [12], near-field focusing plates (NFFPs) [13]. In this paper, we focus on NFFPs and thus propose a novel structure referred to as dual polarized NFFP (DP-NFFP) with focus in two dimensions, being able to provide the field concentration in the two directions parallel to the plate for both polarizations of the illuminating field.

The concepts of achieving optical super-resolution from apertures much smaller than the operating wavelength discussed in [14] resulted in the fundamentals of near-field scanning optical microscopy (NSOM). To overcome the diffraction limit [1], Pendry introduced the general concept of a lens (he called it "perfect lens") made of a flat slab of left-handed material (i.e., a material with negative refractive index) in [3] (the proposed structure is a slab with $\varepsilon = -1$ and $\mu = -1$). This "perfect lens" yields "perfect imaging" by focusing propagating waves as well as supporting growing evanescent waves which restore, at the image plane, the decaying evanescent waves emanating from the source. However, Pendry concluded in [3] that left-handed slabs allow "perfect imaging" if they are completely lossless, impedance matched, and their refractive index is –1 relative to the surrounding medium. Grbic and Eleftheriades proposed simulation [15] and experimental [16] analyses of planar slabs of *L*-*C* loaded transmission line, two-dimensional, left-handed media to support growing evanescent waves to demonstrate imaging beyond the diffraction limit at microwave frequencies.

#154036 - $15.00 USD Received 6 Sep 2011; revised 18 Oct 2011; accepted 20 Oct 2011; published 15 Nov 2011

Subwavelength metallic NFFPs (also known as screens) have been proposed for near-field scanning optical microscopy applications, because they are able to focus the illuminating field into a subwavelength region, or, by reciprocity, selectively collect the field from a subwavelength scatterer [13,17–22]. One of the main advantages of NFFPs over metamaterial lenses (as in [3,15,16]) is that NFFPs are less sensitive to ohmic losses, due to the wave passing through the holes in the screen, and not throughout a region of wave propagation, i.e., the focusing behavior of the screens is mainly insensitive to losses [17]. A metal transmission screen with subwavelength spaced slots has been proposed in [17] with a focus size, in a single direction (perpendicular to the longer sides of the slots and parallel to the plate), of $0.25\lambda_0$ or $0.144\lambda_0$ (where λ_0 is the free space wavelength), for a lens made either of 3 or 9 slots, respectively, at a distance of a quarter wavelength away from the lens, at 10 GHz. In [18], using a patterned grating-like plate consisting of a 1D array of interdigitated capacitors printed on a thin substrate, the electromagnetic near-field focusing of about $0.05\lambda_0$, at a distance of $\lambda_0/15$ from the array, has been achieved in a single direction parallel to the array axis, at 1 GHz. The authors of [19], being inspired by the holography principle, investigated the concept of making simple transmission screens made of three subwavelength slots, in order to achieve a focusing size of $0.2\lambda_0$ in a single direction (perpendicular to the longer sides of the slots and parallel to the plate) at the distance of $0.1\lambda_0$ from the plate, at 3 GHz. A detailed investigation on single-polarized NFFPs made of slotted metallic meta-screens has been studied in [13], for both cases of lenses made of perfect electric conductor (PEC) and silver, at the operating optical frequency of 360 THz, with a focus size of $0.22\lambda_0$ for a plate made of 3-slots and $0.14\lambda_0$ for a plate made of 9-slots in one direction (perpendicular to the longer sides of the slots and parallel to the plate) and at a distance of $0.25\lambda_0$ from the lens. Furthermore, a single-polarized subwavelength focusing plate has been introduced in [20] with focus in two dimensions of $0.27\lambda_0 \times 0.38\lambda_0$ at a distance of $0.25\lambda_0$ from the lens, at 10 GHz.

Recently, in [21], it was shown experimentally at 2.4 GHz that a single-polarized near-field antenna array probe made of three printed passive dipoles was able to perform subwavelength focusing with focus size of $0.235\lambda_0$ in one direction (parallel to the plate and orthogonal to the dipoles) at a quarter wavelength distance from the probe. An analytical approach to model the focusing behavior of the near-field plates made of non-periodic slots was proposed in [22].

A near-field probe fed by a coaxial cable has been proposed in [23] with focusing of $0.217\lambda_0$ in two dimensions (in the plane perpendicular to the field propagation direction) at a quarter wavelength distance from the lens at 2.4 GHz. However, the probe introduced in [23] has been designed to be fed by a coaxial cable which cannot be used at very high frequencies (i.e., optics) and also in planar focusing applications. Furthermore, at optical frequencies, it could be advantageous to retain the possibility to illuminate a planar focusing plate (i.e., a meta-screen as in [13,19–21]) by various possible types of sources.

Field enhancement and subwavelength focusing in near-field have been inspected and achieved at optical frequencies also by exploiting collective resonances in periodic arrays of plasmonic nanoparticles, with subwavelength distance between the constitutive nanoparticles, in one (linear) or two (planar) dimensions, by resonant excitation of surface modes that are characterized by large tangential wave numbers [9,24–26]. For example, in [24], such a possibility was demonstrated with the use of two parallel planar arrays of metal nanospheres. Furthermore, it has been verified, in [9], that the analyzed layered "artificial material" made of two parallel planar arrays of metal nanospheres was able to locate the position of two scatterers with subwavelength separation (e.g., $0.29\lambda_0$, with λ_0 = 380 nm) for a distance of $0.6\lambda_0$ between the observation-plane and the scatterers.

In this work, the proposed DP-NFFP is designed first considering an ideal lossless PEC plate in free space at 193 THz (λ_0 = 1550 nm). Then, a silver plate is analyzed including metal losses, and the results are compared to those of the PEC case, found to be in good agreement in the subwavelength focusing. This shows that the design performance is somehow independent of the material choice and losses at the working near-infrared frequency. The

#154036 - $15.00 USD Received 6 Sep 2011; revised 18 Oct 2011; accepted 20 Oct 2011; published 15 Nov 2011

design procedure is provided in detail. Notice that the DP-NFFP proposed here could be employed from microwave to optical frequencies, thus the design at 193 THz could be easily scaled to other working frequencies: see for example [27] for a DP-NFFP working at 2.4 GHz. In this paper we also introduce the detailed design procedure of this kind of lenses, not mentioned in [27]. We also discuss the limitations of the current design by looking at all the field components. They were not shown in previous studies of similar geometries (e.g [13,17].), and we show here that the clear adavantage of our design, in terms of subwavelength focusing, is achieved only for transverse polarizations, i.e., for electric field polarization parallel to the DP-NFFP. Similar polarization studies should be conducted for previously published geometries. In this paper we confirm the new subwavelength focusing performance by using two independent full-wave simulators, as described in the next paragraph, opening the path to future possible experimenatl results. A DP-NFFP could be employed in near-field optical microscopy applications and could allow for object-detection independent of position of a sample located in either of the axes in the plane of the lens (i.e., there is no need of tip-rotation in microscopy); furthermore, it could allow for object-detection independent of polarization of the illuminated wave (i.e., some scatterers are detectable only for a specific field polarization).

The structure of the paper is as follows. The design procedure is presented in Sec. 2, where a working set of dimensions for the proposed lens is provided for a DP-NFFP that shows subwavelength focusing performance for two polarizations, in two dimensions, comparable to what was achieved in previous studies in only one dimension for one polarization [13,17]. Further improvement may be obtained by using optimization algorithms. The focusing properties of the proposed design are discussed in Sec. 3, where the structure is also compared to the single subwavelength square hole in a metallic plate. The focusing dependence with respect to the operational frequency of the proposed structure is also shown. The limitations of the proposed design are discussed.

2. Design procedure

To guide the reader through the understanding of the basic principles of the proposed structure we start with the dual polarized structure (by symmetry) shown in Fig. 1(a); it is a metallic plate with a cross shaped central hole and two lateral slots in both the *x*- and *y*-directions. In general, the metal plate is embedded in a homogeneous background with permittivity ε_h, or it can be placed on a substrate material and/or covered by a dielectric cover layer (i.e., source and focusing half spaces may be made of different materials).

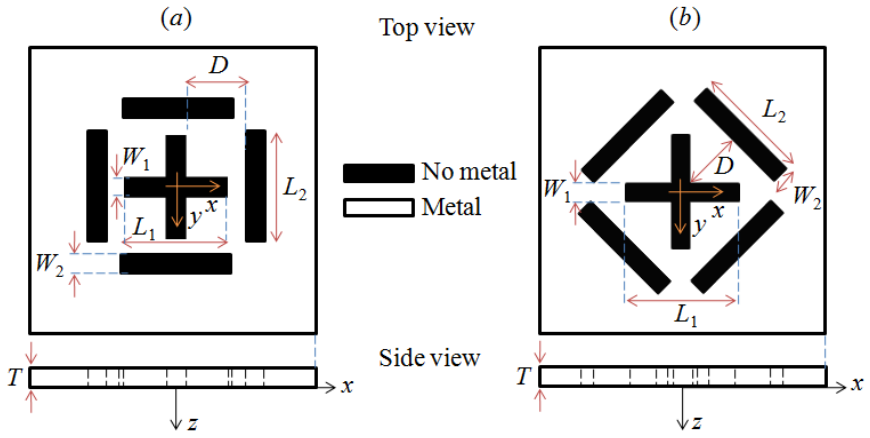

Fig. 1. The top and side views of the DP-NFFP structure with dimensions. (a) The initial design,and (b) the design with improved focusing.

#154036 - $15.00 USD Received 6 Sep 2011; revised 18 Oct 2011; accepted 20 Oct 2011; published 15 Nov 2011

In this work, all the designs are based on homogeneous background with $\varepsilon_h = 1$. The length of the central cross L_1 (kept equal in both *x*- and *y*-directions for symmetry reasons) is selected equal to its resonance length at the designed frequency of 193 THz (1550 nm), whereas the length of the lateral slots L_2 (again kept equal in both *x*- and *y*-directions for symmetry reasons) is selected a bit shorter than the resonance length of the lateral slots, as explained in Sec. 2.4. The widths of the cross shaped hole and of the lateral slots, W_1 and W_2, and the thickness of the plate T are fixed to 60 nm for all the sections throughout this work (this will be valid for the two structures shown in Fig. 1) in order not to have too small slot widths that would be hard to fabricate. The subwavelength focusing of the proposed DP-NFFP can be explained by the presence of strong evanescent waves (near field components) that produce fields that decay rapidly away from the cross and slot elements, leading to a coherent localization of fields at a certain distance from the plate, as mentioned in [17], for example. Performance of a PEC DP-NFFP has been analyzed in this section with the full-wave simulator CST Microwave Studio (time domain), with the "open" boundary condition, assuming plane wave illumination.

2.1. Determination of the resonant dimensions for the cross central element

The first step consists in the computation of the resonant length $L_1 = L_{CR}$ of the cross central hole, as mentioned in the previous part. The procedure is shown in Fig. 2(a). The plate is illuminated with a plane wave from the top half space with electric field magnitude of 1 V/m polarized along *x*. Then, the magnitude of the *x*-component of the transferred electric near-field $|E_T|$ on the *z*-axis, at $x = y = 0$ (the coordinate system is placed in the center of the lens as shown in Fig. 2(a)), at positions $z = 0.15\lambda_0, 0.2\lambda_0, 0.25\lambda_0$ in the focusing bottom half space, is calculated for different L_1 values and plotted in Fig. 2(b). We look for the length value for L_1 that maximizes $|E_T|$, which is achievable when the cross resonates, which results in $L_1 = L_{CR} = 750\,\text{nm}$.

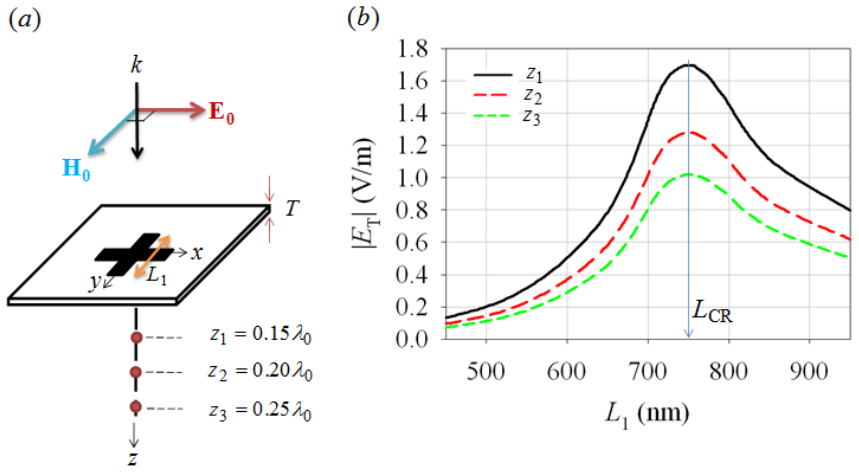

Fig. 2. (a) Schematic for the resonance length determination procedure for the central cross shaped hole, and (b) the relative electric field magnitude plot at different distances from the plate, as outlined in part (a), simulated with CST.

2.2. Determination of the resonant dimensions for the lateral slots

The second tuning step consists in the computation of the resonant size $L_2 = L_{SR}$ of the lateral slots. The procedure is shown in Fig. 3(a). The plate is again illuminated with a plane wave

#154036 - $15.00 USD Received 6 Sep 2011; revised 18 Oct 2011; accepted 20 Oct 2011; published 15 Nov 2011

from the top half space with electric field magnitude of 1 V/m polarized along *x*; the magnitude of the *x*-component of the transferred electric near-field $|E_T|$, calculated at *x* = *y* = 0, and at $z = 0.15\lambda_0, 0.2\lambda_0, 0.25\lambda_0$, is found for different L_2 values, and plotted in Fig. 3(b). Again, we look for the length value L_2 that maximizes $|E_T|$, which is achievable when the slot resonates, which results in $L_2 = L_{SR} = 725\,\text{nm}$.

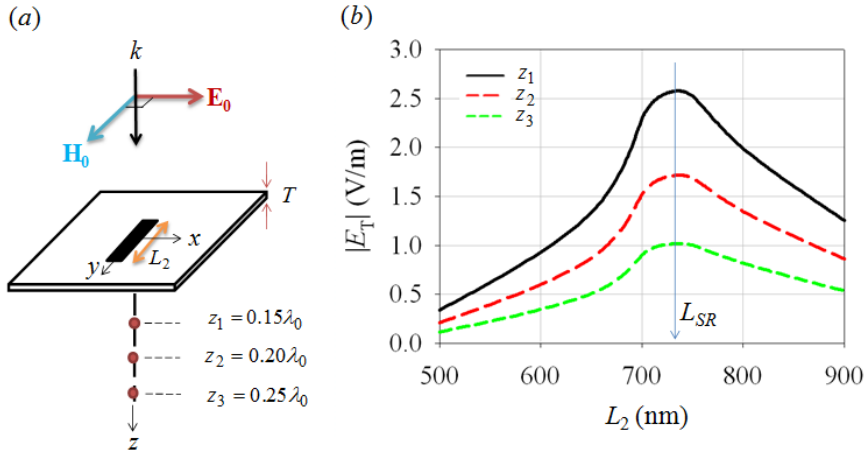

Fig. 3. (a) Schematic for the resonance length determination procedure for the lateral slots, and (b) the relative electric field magnitude plot at different distances from the plate, as outlined in part (a), simulated with CST.

2.3. Definition of two figures of merit for focusing structures

Before continuing with the design procedure description it is useful to introduce the two figures of merit discussed next.

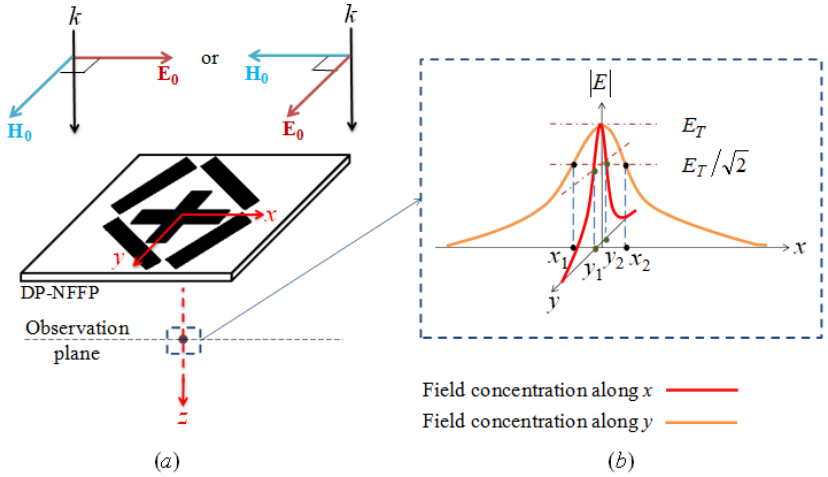

Fig. 4. Schematic for the definition of the figures of merit of the lensing structure. (a) DP-NFFP illuminated by *x*-polarized (or *y*-polarized) plane-wave. (b) The magnitude of the *x*-component (or *y*-component) of the focused electric near-field at a certain distance below the DP-NFFP (observation plane), and *FWHM* in each dimension.

#154036 - $15.00 USD Received 6 Sep 2011; revised 18 Oct 2011; accepted 20 Oct 2011; published 15 Nov 2011

2.3.1. Field transfer ratio F

According to Fig. 4, the plate is illuminated with a plane wave from the top half space with electric field $\mathbf{E}_0 = E_0\hat{\mathbf{s}}$, with $\hat{\mathbf{s}}$ being either $\hat{\mathbf{x}}$ or $\hat{\mathbf{y}}$. Accordingly, focusing of the transferred electric near-field in the bottom half plane will be along both $\hat{\mathbf{x}}$ or $\hat{\mathbf{y}}$, with magnitude $|E_T|$. Then, the field transfer ratio is defined as

$$F = \left|\frac{E_T}{E_0}\right| \times 100\%, \tag{1}$$

where *F* represents the percentage of the illuminated field that passes through the lens.

2.3.2. Full width half maximum (FWHM) in each direction

The *FWHM* is determined as the absolute value of the difference between the two positions at which $|E_T|^2$ is one half of its maximum. According to Fig. 4, we define the *FWHM* along *x*- and *y*-directions as

$$FWHM_x = |x_2 - x_1|, \qquad FWHM_y = |y_2 - y_1|. \tag{2}$$

As a rule of thumb, the larger the distance from the plate, the larger the *FWHM* of the DP-NFFP (i.e., focusing becomes worst with further distances).

2.4. Final design step

There is a trade-off between the field transfer ratio *F* and the *FWHM* of the lens; therefore, the dimensions of the lens can be optimized to achieve desired features. Here, an intermediate situation between reducing the *FWHM* of the focused field and increasing the field transfer ratio is designed. The aim is to show that a DP-NFFP with focusing in two dimensions is obtainable, though further improvement could be achieved by optimization.

The dimensions of the initial design in Fig. 1(a) made of a PEC plate are as follows: thickness $T = 60\,\text{nm}$, with the central cross hole having dimensions L_1 to be determined and $W_1 = 60\,\text{nm}$, lateral slots having dimensions L_2 to be determined and $W_2 = 60\,\text{nm}$, and $D = 390\,\text{nm}$. The lens is embedded in a homogeneous background with relative permittivity $\varepsilon_h = 1$ (i.e., free space). The minimum spatial feature of around 40 nm (i.e., the minimum distance of 42.5 nm between the cross and the lateral slots) has been chosen to meet the current fabrication standards. However, we have observed that smaller distances would slightly improve focusing (as shown in Sec. 2.5).

The final design step consists in observing the focusing behavior of the structures obtained by combining lengths $L_1 = L_{CR} \pm \delta$ and $L_2 = L_{SR} \pm \delta$, resulting in nine different designs. We fixed $\delta = 75\,\text{nm}$, and the normalized near-field intensity (with respect to its maximum) is plotted versus the normalized *x* and *y* coordinates (with respect to λ_0), at the fixed distance $z = 0.25\lambda_0$ from the plate, for *x*-polarized wave illumination, in Figs. 5 and 6, respectively.

Looking at the designs analyzed in Fig. 5, it can be observed that for the case outlined in Fig. 5(d), in which $L_1 = L_{CR}$ and $L_2 = L_{SR} - \delta$, the lens shows the best focusing behavior (i.e., minimum $FWHM_x$ for the chosen δ) of $0.238\lambda_0$ along the *x*-axis. However, the same structure cannot provide a focusing behavior on the *y*-axis (see Fig. 6(d)) comparable to the aforementioned result along the *x*-axis. Notice that in the case outlined in Fig. 6 the lens shows the best focusing behavior (i.e., minimum $FWHM_y$ for the chosen δ) of $0.296\lambda_0$ along the *y*-axis in the design in Fig. 6(c), in which $L_1 = L_{CR} - \delta$ and $L_2 = L_{SR} + \delta$. Therefore, the mentioned structure is able to provide a subwavelength focusing behavior for both *x*- and *y*-polarization with a focusing comparable to what it has been published so far *only* in one

#154036 - $15.00 USD Received 6 Sep 2011; revised 18 Oct 2011; accepted 20 Oct 2011; published 15 Nov 2011

direction (e.g., if we choose structure (d) which has $L_1 = L_{CR}$ and $L_2 = L_{SR} - \delta$, for an *x*-polarized plane-wave illumination, an acceptable focusing (compared to what has been published) is achieved for the *x*-direction only).

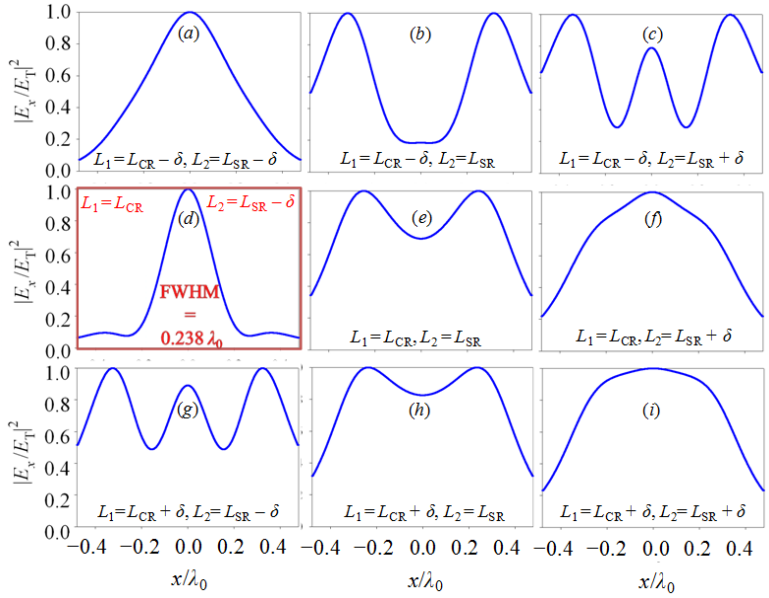

Fig. 5. The nine designs for the proposed structure in Fig. 1(a). Field E_x observed moving along the *x*-direction, for *x*-polarized wave illumination, at a distance of $0.25\lambda_0$ from the lens, simulated with CST.

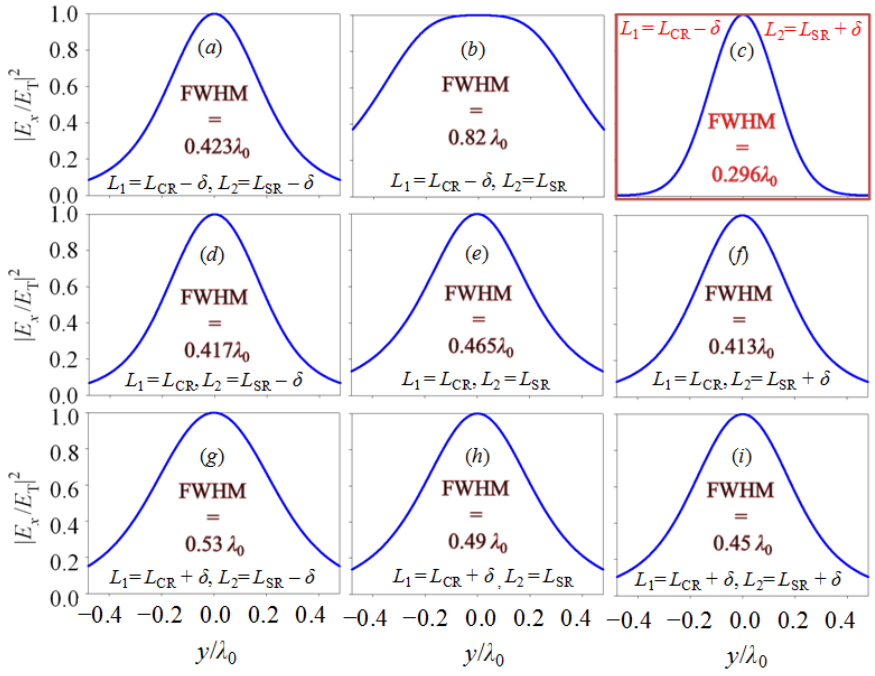

Fig. 6. As in Fig. 5, but field E_x observed moving along the *y*-direction.

#154036 - $15.00 USD Received 6 Sep 2011; revised 18 Oct 2011; accepted 20 Oct 2011; published 15 Nov 2011

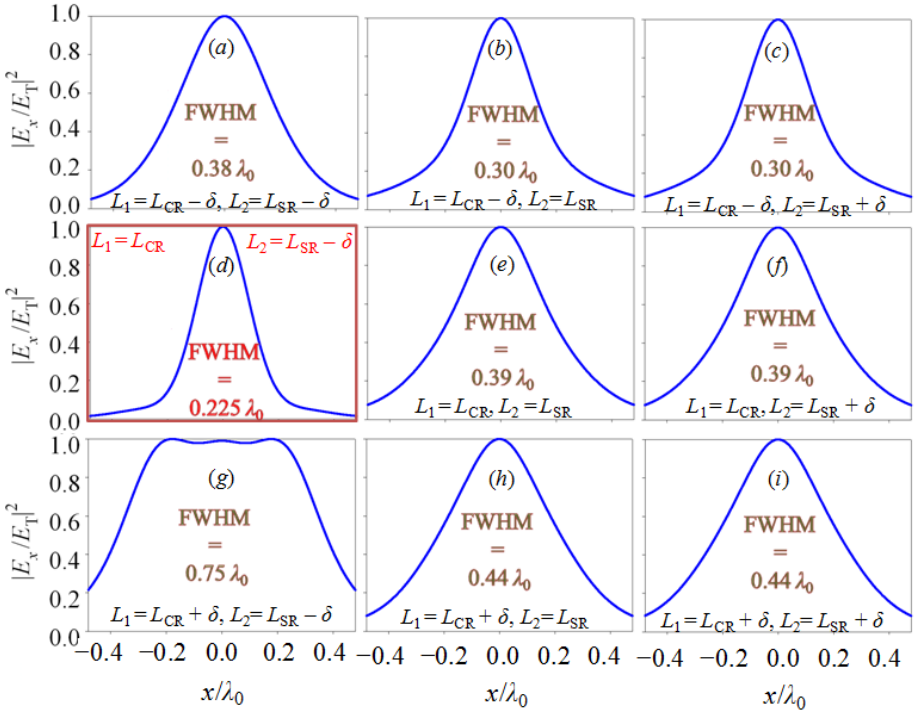

Fig. 7. The nine designs for the proposed DP-NFFP in Fig. 1(b). Field E_x is observed moving along the *x*-direction, for *x*-polarized illuminating wave, at a distance of $0.25\lambda_0$ from the lens, simulated with CST.

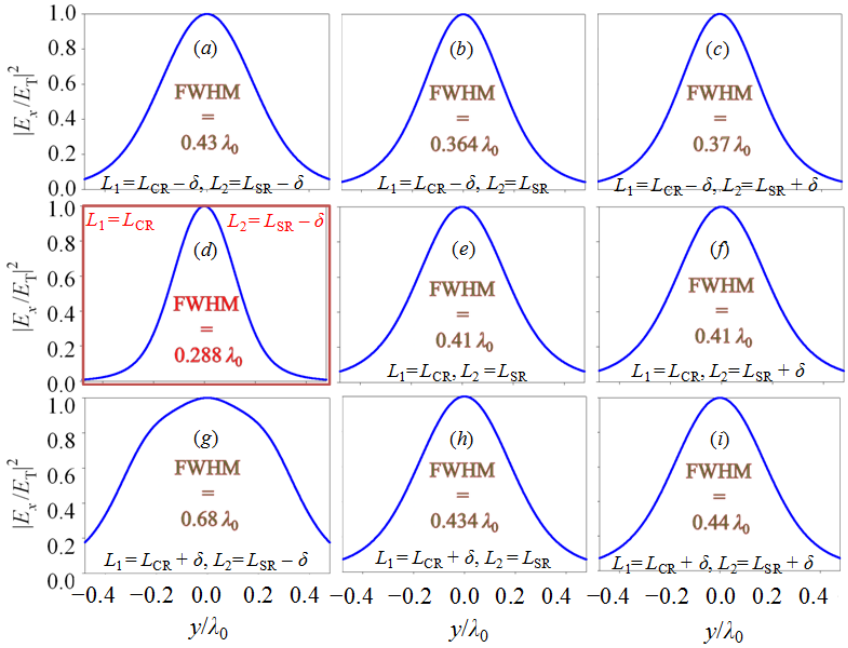

Fig. 8. As in Fig. 7, but field E_x observed moving along the *y*-direction.

#154036 - $15.00 USD Received 6 Sep 2011; revised 18 Oct 2011; accepted 20 Oct 2011; published 15 Nov 2011

The same behavior has been obtained for *y*-polarized wave illumination (case not shown for the sake of brevity) where, due to the symmetry of the problem, the better focus is achieved in the *y*-axis instead of the *x*-axis for the design in which $L_1 = L_{CR}$ and $L_2 = L_{SR} - \delta$. Because of the symmetry of the designed DP-NFFP only results relative to the *x*-polarized illumination case are shown.

We have observed that the rotation of the lateral slots in the design in Fig. 1(a) by 45 degrees with respect to the central cross shaped hole, as shown in Fig. 1(b), allows for improved focusing along both *x*- and *y*-directions, for both polarizations, with respect to the structure in Fig. 1(a).

Moreover, notice that by rotating the lateral slots, the minimum distance between the central cross and the lateral slots is increased with respect to the case in Fig. 1(a). Thus, to maintain the minimum distance of 42.5 nm between the holes in the structure shown in Fig. 1(b) for ease of fabrication (to be kept equal to the one in Fig. 1(a)), *D* is selected equal to 325 nm. Therefore, the design procedure outlined in Sec. 2 is applied again to the structure in Fig. 1(b), and the nine designs are shown in Figs. 7 and 8, with $\delta = 75\,nm$. It can be observed that, for the lens with $L_1 = L_{CR}$ and $L_2 = L_{SR} - \delta$ presented in Figs. 7(d) and 8(d), the subwavelength focusing is the minimum between all the nine configurations, and equal to $0.225\lambda_0$ and $0.288\lambda_0$ in the *x*- and *y*-axis, respectively, for *x*-polarization. Analogous results are obtained for *y*-polarized incident plane wave (not shown to avoid repetition). The reported parameterization clearly shows that a DP-NFFP with focusing of the transverse polarization, in two dimensions, is achievable, though a further improvement could be obtained by using optimization algorithms.

2.5. Focusing behavior for different distances D between the central and the lateral slots

Figure 9 shows a comparison between the normalized field concentration intensities along both the *x*- and *y*-axis due to an *x*-polarized field illumination, for lenses with different values of *D* (all the other parameters are kept equal to the ones in Sec. 2.4 for the DP-NFFP in Fig. 1(b)).

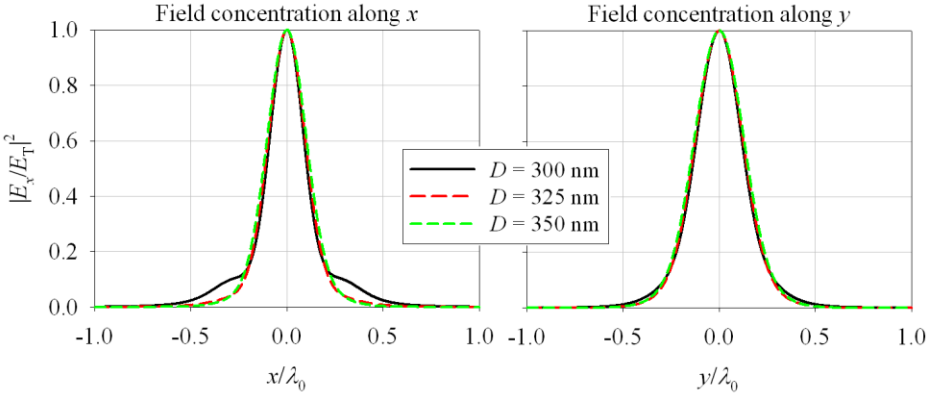

Fig. 9. Normalized near-field intensities for various *D* values (Fig. 1(b)) along the *x*- and *y*-direction, at a distance of $0.25\lambda_0$ from the lens, due to an *x*-polarized field illumination, simulated with CST.

For smaller values of *D* (i.e., shorter distance between the central cross hole and the lateral slots), the focusing is just slightly improved. This result mainly shows that it is not necessary to choose the smallest value of *D*, which would not only limit the performances due to the presence of higher side lobes, but also affect the minimum geometrical feature of the structure, i.e., the minimum distance between the holes in the plate, which is 7 nm for *D* = 300 nm, 42.5 nm for *D* = 325 nm, and 78 nm for *D* = 350 nm for the design in Fig. 1(b). In

#154036 - $15.00 USD Received 6 Sep 2011; revised 18 Oct 2011; accepted 20 Oct 2011; published 15 Nov 2011

summary, the modification of this parameter does not impact much in the overall performance of the proposed DP-NFFP design. However, the variation of *D* combined to the variation of other design parameters could be exploited by using optimization algorithms.

3. DP-NFFP properties and discussion

In this section, the DP-NFFP performance has been analyzed with two full-wave simulators, i.e., Ansys HFSS (frequency domain finite elements method) and CST Microwave Studio (time domain): in the HFSS simulations, the lens is surrounded by periodic boundaries, modeling a two dimensional periodic array of DP-NFFPs, with unit cell size equal to λ_0, illuminated by a plane wave (more explanations and result dependence on the unit cell size are provided in the Appendix A); the CST simulation setup is as described in Sec. 2 (i.e., with open boundary condition).

3.1. Comparison between a single square hole and the proposed DP-NFFP

We compare the normalized near-field intensity of the focused field on the observation plane at $z = 0.25\lambda_0$ (see Fig. 4(a)), transmitted by both the proposed DP-NFFP in Fig. 1(b) and by a plate with a single subwavelength square hole (see insets in Fig. 10). Full-wave simulation results obtained by using both CST and HFSS, Fig. 10, agree on the width and shape of the field focused by the DP-NFFP. According to these simulations, the field transfer ratio *F* for the DP-NFFP (taken from CST in case of plane wave illumination) is approximately 53%. In order to make a significant comparison, the square hole is chosen to have a lateral size of $0.33\lambda_0$ such that it provides the same field transfer ratio *F* (and thus the same transmitted field E_T) as the proposed DP-NFFP shown in Fig. 1(b). A far better near-field subwavelength focusing behavior with respect to the square hole is observed for the proposed DP-NFFP. In particular, for the case of a single square hole plate, for an *x*-polarized field illumination, we have $FWHM_x = 0.4\lambda_0$ and $FWHM_y = 0.37\lambda_0$, respectively, whereas the proposed DP-NFFP design achieves $FWHM_x = 0.225\lambda_0$ and $FWHM_y = 0.288\lambda_0$, respectively (taken from CST curves). The general agreement between HFSS and CST results in predicting the near-field focusing cross validates the claim that the proposed structure is able to provide subwavelength focusing in two dimensions.

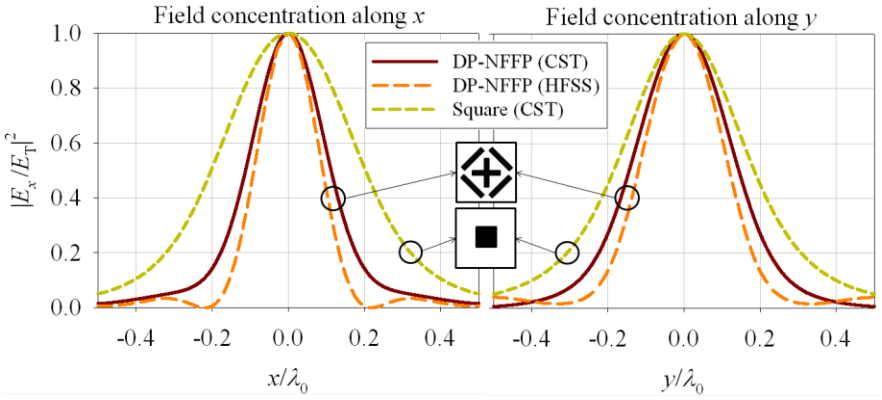

Fig. 10. Normalized near-field intensities at a distance of $0.25\lambda_0$ from the lens for the proposed DP-NFFP and a single square hole plate. The proposed DP-NFFP exhibits a much better near-field subwavelength focusing in both the *x*- and *y*-directions, for both HFSS and CST full-wave simulation results.

#154036 - $15.00 USD Received 6 Sep 2011; revised 18 Oct 2011; accepted 20 Oct 2011; published 15 Nov 2011

3.2. Focusing versus distance from the plate

The normalized (with respect to the maximum of the *x*-component of the transferred electric near-field, E_T) field concentration intensity of the lens on both *x*- and *y*-axis is shown in Fig. 11 at 193 THz (1550 nm), for an *x*-polarized plane-wave illumination and for different observation distances from the plate. It can be seen that the *FWHM* of the lens increases (i.e., worst focusing) by getting farther from the structure. The *FWHM* of the lens at the focusing distance of $0.15\lambda_0$ from the plate is about $0.15\lambda_0$ and $0.24\lambda_0$ on the *x*- and *y*-axis, respectively. At a distance of $0.2\lambda_0$ from the DP-NFFP, the *FWHM* is approximately equal to $0.185\lambda_0$ and $0.256\lambda_0$ on the *x*- and *y*-axis, respectively. At a distance of $0.25\lambda_0$, the *FWHM* is approximately equal to $0.225\lambda_0$ and $0.288\lambda_0$ along the *x*- and *y*-axis, respectively.

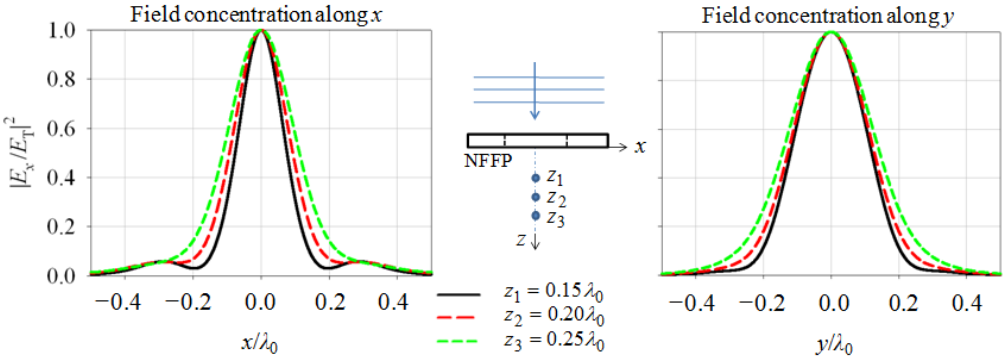

Fig. 11. Normalized field concentration intensity at 193 THz produced by the proposed DP-NFFP in Fig. 1(b) on both *x*- and *y*-direction due to an *x*-polarized plane-wave at different *z*-distances, simulated with CST.

The field transfer ratio *F* decreases, as expected, by getting farther from the DP-NFFP. For focusing distances equal to $0.15\lambda_0$, $0.2\lambda_0$ and $0.25\lambda_0$, *F* is around 102%, 70% and 53%, respectively.

Table 1 shows a comparison summary for the proposed DP-NFFP in Fig. 1(b) (with cross + lateral slots), and two other simpler plates made by (i) the cross only (without the lateral slots), and (ii) a subwavelength square hole, assuming an *x*-polarized plane wave illumination, and observing at $0.15\lambda_0$, $0.2\lambda_0$ and $0.25\lambda_0$ from the plate. Results are from CST simulations. The square hole size was selected in order to provide the same field transfer ratio as in the proposed design in Fig. 1(b) (i.e. square holes with $L = 0.37\lambda_0$, $0.34\lambda_0$ and $0.33\lambda_0$ have the same *F* as the one for the designed structure, shown in Fig. 1(b), at distances of $0.15\lambda_0$, $0.2\lambda_0$ and $0.25\lambda_0$ from the lens, respectively).

Table 1. Comparison of the Performance of Different Screens

DP-NFFPs	Focusing direction	At $z = 0.15\lambda_0$		At $z = 0.2\lambda_0$		At $z = 0.25\lambda_0$	
		FWHM (λ_0)	*F* (%)	FWHM (λ_0)	*F* (%)	FWHM (λ_0)	*F* (%)
DP-NFFP	*x*	0.15	102	0.18	70	0.22	53
cross only		0.20	170	0.26	128	0.33	102
square hole		0.37	102	0.38	70	0.40	53
DP-NFFP	*y*	0.24	102	0.26	70	0.29	53
cross only		0.31	170	0.34	128	0.39	102
square hole		0.29	102	0.32	70	0.37	53

#154036 - $15.00 USD Received 6 Sep 2011; revised 18 Oct 2011; accepted 20 Oct 2011; published 15 Nov 2011

It can be seen from Table 1 that, as expected, the *FWHM* of the proposed DP-NFFP is improved thanks to the use of the lateral slots when compared to the case with only a single cross. Also, the designed DP-NFFP has a much better focusing behavior in comparison with a single square hole, assuming they both provide the same field transfer ratio *F*.

3.3. Limitations of the proposed design: Analysis of the components of the focused field

In this part, we discuss the limitations of the proposed design by looking at all the field components in the focusing area, for the structures in Figs. 1(a) and 1(b), and the square hole geometry analyzed in Sec. 3.1.

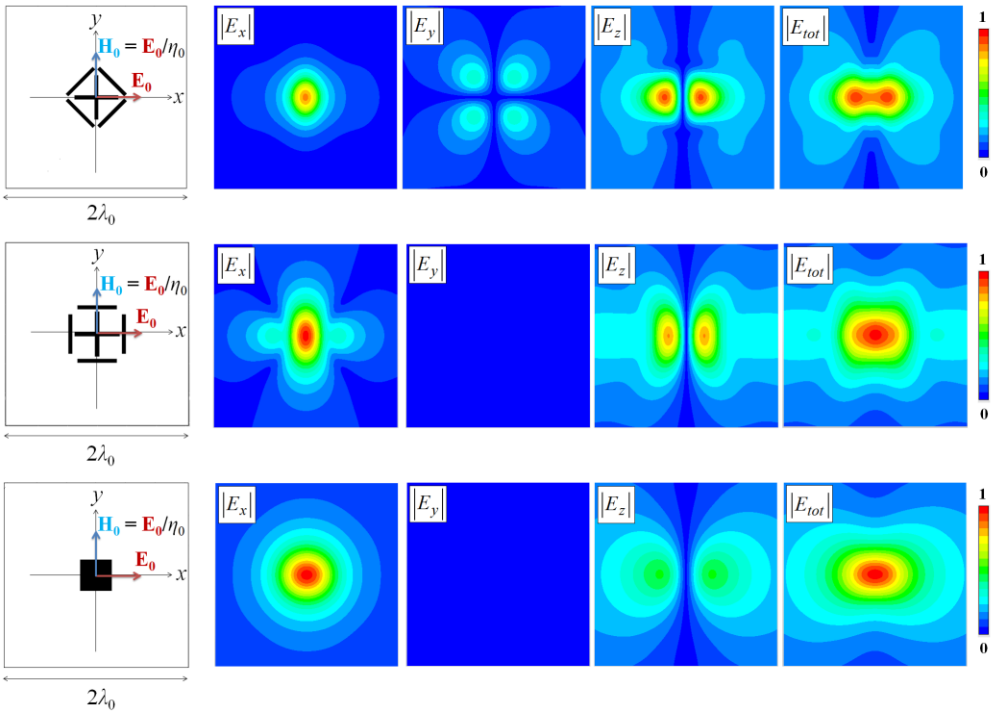

Fig. 12. Field maps evaluated at $z = 0.25\lambda_0$ showing the normalized magnitude of the field components and total field (with respect to the maximum value of the total field for each structure) due to an *x*-polarized plane-wave illumination, simulated with CST. The first configuration (i.e., the DP-NFFP in Fig. 1(b)) shows better focusing of the transverse (*x*,*y*)-field components.

The magnitude field maps, due to an *x*-polarized plane-wave illumination, are reported in Fig. 12, normalized with respect to the maximum value of the total field for each structure. Note that in all the analyzed lenses, the *y*-component of the field is negligible with respect to the *x*- or *z*-components. Moreover, the *z* component has two peaks, producing a deterioration of the focusing performance when looking at the total field, in all the three designs. Since in this study we wanted to show that the transverse field components can be focused in two dimensions and for both polarizations, to be compared to previous analogous studies [13,17] that show focusing of the transverse field in one dimension only, the total field was not considered in the design procedure in Sec. 2. Improvement of the design considering also the *z* polarized field will be studied in the future.

3.4. Model investigation for the realistic case of a plate made of silver (Drude model)

In this part, the properties of the proposed DP-NFFP in Fig. 1(b) are observed in the case of a plate made of silver at 193 THz (1550 nm). At optical frequencies, losses assume an

#154036 - $15.00 USD Received 6 Sep 2011; revised 18 Oct 2011; accepted 20 Oct 2011; published 15 Nov 2011

important role that impacts in the overall characteristics of the analyzed structure. Silver relative permittivity at optical frequencies is modeled by using the Drude model as $\varepsilon_m = \varepsilon_\infty - \omega_p^2 / \left\lfloor \omega(\omega - j\gamma) \right\rfloor$, where ω_p is the plasma angular frequency, γ is the Drude damping term, and ε_∞ is a high frequency fitting parameter used to match experimental results, such as the ones reported in [28]. The parameters related to the Drude model, based on the information provided in [29,30] for silver, are $\varepsilon_\infty = 5$, $\omega_p = 1.37 \times 10^{16}$ rad/s, and $\gamma = 27.3 \times 10^{12}$ s^{-1}.

Figure 13 shows a comparison between full-wave simulations of the normalized field concentration intensity along the *x*- and *y*-directions, due to an *x*-polarized field illumination, of the designed DP-NFFP shown in Fig. 1(b), made either by PEC or by silver. It can be seen that both ideal (PEC) and realistic (silver) metal plates provide with comparable subwavelength focusing. For this reason, two important facts can be outlined: (i) the focusing is not affected significantly by the presence of the losses that arise in the metal at the analyzed infrared frequency and (ii) the stability with respect to the material losses let us conclude that the DP-NFFP is feasible with a real material.

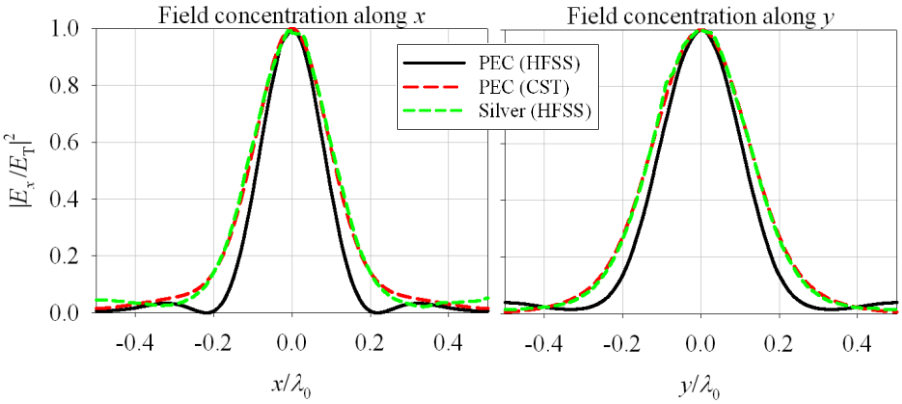

Fig. 13. Normalized field intensities of the designed DP-NFFP made either by silver or PEC, along the *x*- and *y*-directions, due to an *x*-polarized plane-wave illumination, at the distance of $0.25\lambda_0$.

3.5. Focusing versus operational frequency

The subwavelength focusing of the DP-NFFP in Fig. 1(b), made of PEC, is investigated varying frequency, here chosen equal to 183 THz (1640 nm), 193 THz (1550 nm), and 203 THz (1480 nm). All the simulations are performed with CST. The normalized field intensity (with respect to the maximum of the *x*-component of the transferred electric near-field, E_T) in both *x*- and *y*-directions is shown in Fig. 14 due to an *x*-polarized plane-wave illumination (propagating normally to the lens) at a distance $z = 0.25\lambda_0$ from the DP-NFFP, where λ_0 is the wavelength at the central frequency of 193 THz. The lens in Fig. 1(b) has been designed to work at 193 THz, at which the narrowest focusing has been achieved, as can be confirmed in Fig. 14; observe that the focusing is worst at 183 THz (but still subwavelength), whereas at 203 THz is even comparable to the wavelength.

As discussed in Secs. 2.1 and 2.2, the focusing properties of the DP-NFFP are based on the lengths of both cross and lateral slots. In particular, the central cross length has been designed to be equal to its resonance length, whereas the lateral slots lengths have been designed to be slightly smaller than their resonance length to achieve subwavelength focusing in two dimensions (Figs. 7 and 8). Notice that the behavior in Fig. 14 can be explained by observing that by changing frequency the lens design scales to one of the other eight

#154036 - $15.00 USD Received 6 Sep 2011; revised 18 Oct 2011; accepted 20 Oct 2011; published 15 Nov 2011

configurations outlined in Figs. 7 and 8, which all provide worse focusing. This confirms that the DP-NFFP exhibits the minimum *FWHM* at its designed frequency of 193 THz.

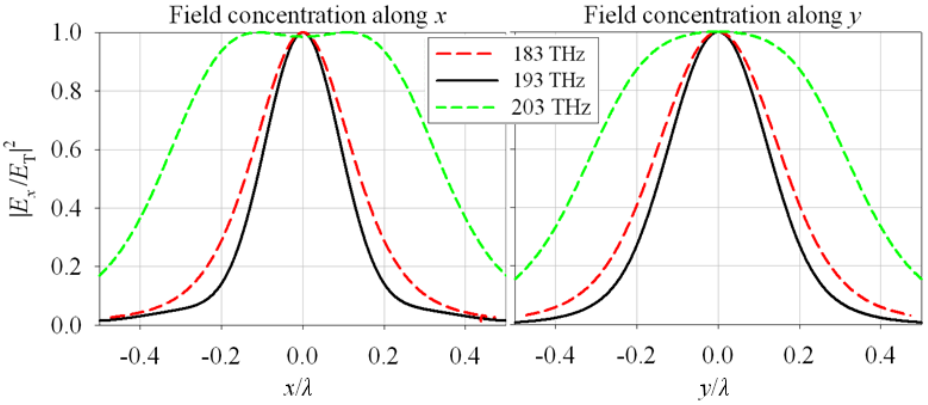

Fig. 14. Normalized field intensities of the designed DP-NFFP moving the observer either along the *x*- or *y*-direction, for three different frequencies, and *x*-polarized wave illumination, simulated with CST. In the plots, λ is the wavelength of the analyzed operating frequency.

4. Conclusion

A novel dual polarized near-field focusing plate (DP-NFFP) has been introduced to operate at the near-infrared frequency of 193 THz (1550 nm). The detailed design steps have been discussed and the simulation results have been verified by both HFSS and CST for the ideal case of DP-NFFP made of PEC, and for the realistic case of DP-NFFP made of silver. The stability of the results based on the PEC and silver simulations let us to conclude that the DP-NFFP design is feasible with real materials. In the present study we kept the design minimum feature to be at least 42.5 nm, with slot width equal to 60 nm. This work has to be seen as an introduction for a dual polarized lens with focus in two dimensions. It is informative in the sense that we discuss the focusing of the transverse components of the field, parallel to the lens, showing a subwavelength performance in two dimensions, for two polarizations, comparable to what has been done previously for one dimension and for one polarization. We also discuss the limitations of the current design by showing the worst focusing of the field component orthogonal to the DP-NFFP, compared to the transverse ones. Using optimization methods, investigations may be carried out to further minimize the *FWHM* and maximize *F* (the amount of field transmitted) at a farther focusing distance. The results shown are in free space and, as customary in microscopy, focusing and resolution can be improved by embedding the DP-NFFP in a liquid or using a dielectric substrate.

Appendix A: using HFSS simulations with periodic boundaries, and coupling effect

The effect on the focusing behavior of the DP-NFFP due to the use in HFSS of "periodic" boundaries (i.e., perfect electric/magnetic conductors, PEC/PMC) along *x* and *y* (which is equivalent to model a two dimensional array of lenses) illuminated by a plane wave is investigated here and the result is compared to the one of the structure simulated by CST, using "open" boundaries, still illuminated by a plane wave.

Figure 15 shows the normalized $|E_x|^2$ field intensity of the lens along both *x*- and *y*-axis due to an *x*-polarized plane wave illumination at the distance $z = 0.25\lambda_0$ from the lens. It can be seen that for increasing *C* (where *C* is the transverse size of the unit-cell, along *x* and *y*, of the proposed structure surrounded by periodic boundaries in the HFSS simulations), the main field-spot of the focused field obtained from HFSS simulations is almost invariant; however, note the arise of small side lobes in the results obtained with HFSS (which are still small and comparable to the level of CST result). These small variations can be attributed to numerical

#154036 - $15.00 USD Received 6 Sep 2011; revised 18 Oct 2011; accepted 20 Oct 2011; published 15 Nov 2011

inaccuracies or to the periodic boundary conditions (and thus to the coupling to virtual adjacent lenses).

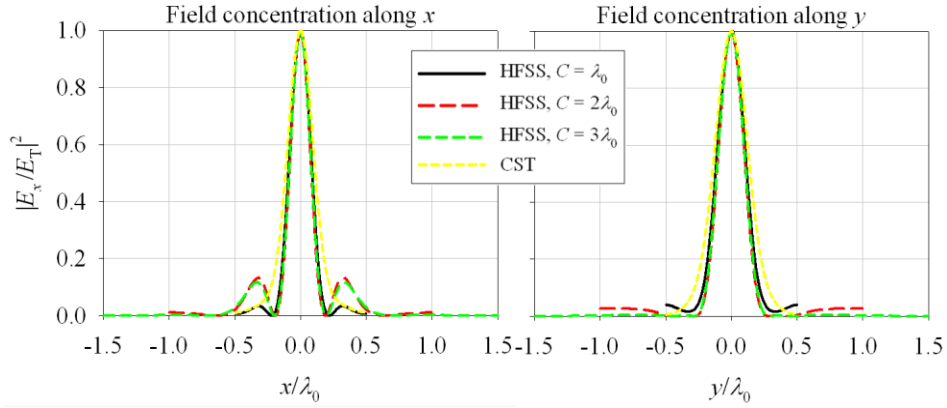

Fig. 15. Normalized field intensity along both *x*- and *y*-directions due to an *x*-polarized plane-wave for a two dimensional periodic array of lenses for different unit-cell size *C*, at the distance $z = 0.25\lambda_0$ from the lens, when simulated with HFSS. Also, the same quantity for a single lens simulated with CST (assuming a plate of infinite extent) is used for comparison.

Acknowledgments

The authors are thankful to Prof. Ozdal Boyraz and Mr. Caner Guclu, University of California Irvine, CA, for useful discussions, and to Computer Simulation Technology (CST) and Ansys (HFSS) for providing their simulation tools that were instrumental in this analysis.

#154036 - $15.00 USD Received 6 Sep 2011; revised 18 Oct 2011; accepted 20 Oct 2011; published 15 Nov 2011